

Superhumps: Confronting Theory with Observation

K. J. Pearson

Louisiana State University, Department of Physics and Astronomy, Nicholson Hall, Baton Rouge, LA 70803-4001, USA.

Accepted . Received ; in original form

ABSTRACT

We review the theory and observations related to the “superhump” precession of eccentric accretion discs in close binary systems. We agree with earlier work, although for different reasons, that the discrepancy between observation and dynamical theory implies that the effect of pressure in the disc cannot be neglected. We extend earlier work that investigates this effect to include the correct expression for the radius at which resonant orbits occur. Using analytic expressions for the accretion disc structure, we derive a relationship between the period excess and mass-ratio with the pressure effects included. This is compared to the observed data, recently derived results for detailed integration of the disc equations and the equivalent empirically derived relations and used to predict values for the mass ratio based on measured values of the period excess for 88 systems.

Key words: stars: binaries: close – stars: novae: cataclysmic variables – stars: dwarf novae – accretion, accretion discs

1 INTRODUCTION

Cataclysmic Variables (CVs) are a class of close binary system, with a typical orbital period of a few hours, where a white dwarf primary accretes material from its companion via Roche lobe overflow. The secondary is normally a late-type main sequence star although examples with an evolved companion do exist (eg. GK Per). In the absence of a significant white dwarf magnetic field, material arrives at the primary after processing through an accretion disc. The dwarf nova subgroup show outbursts where the luminosity of the system increases by around 2–5 mag. Although not strictly periodic, these recur on a typical timescale for each system ranging from tens of days to tens of years. The dwarf novae are further subdivided based on the properties of the outbursts. We will be interested in the SU UMa type where the systems show occasional superoutbursts which have a brighter maximum (~ 0.7 mag.) and longer duration (~ 5 times) than normal outbursts.

The most favoured explanation for dwarf nova outbursts involves an ionization instability where the accretion disc mass increases until a critical surface density

$$\Sigma_{\max} = 114 \text{ kg m}^{-2} \left(\frac{r}{10^8 \text{ m}} \right)^{1.05} M_1^{-0.35} \alpha_C^{0.86} \quad (1)$$

is reached at some radius r . When this occurs, the disc switches into a “hot” state with higher viscosity that causes a larger mass transport rate through the disc and increased luminosity. The disc mass now steadily decreases until a second critical surface density

$$\Sigma_{\min} = 82.5 \text{ kg m}^{-2} \left(\frac{r}{10^8 \text{ m}} \right)^{1.05} M_1^{-0.35} \alpha_H^{0.8} \quad (2)$$

is reached at some point. Upon meeting this condition, the disc transfers back to the “cold” quiescent state and the cycle repeats. In these expressions α_C and α_H are the Shakura-Sunyaev viscosity parameters in the cold and hot states respectively and the primary mass M_1 is measured in solar masses (Cannizzo, Shafter & Wheeler 1988).

SU UMa superoutbursts also have the property of showing superhumps. Here, an additional periodicity (P_{sh}) a few percent longer than the orbital period (P_{orb}) is apparent in the lightcurve. This is believed to arise from a precessing, eccentric accretion disc driven by a resonance between the orbiting disc material and the secondary. CVs in general and the SU UMa systems in particular are well-reviewed by Warner (1995). Some systems other than dwarf novae also show superhumps which, by analogy, are believed to share a common origin with an eccentric disc now permanently present giving rise to “permanent superhumps” (Retter & Naylor 2000). Similarly, some Low-Mass X-ray Binaries (LMXBs); analogues to CVs where the primary is now a neutron star, have also been discovered to have superhumps eg. KV UMa (Zurita et al. 2002). There is also a related phenomenon of “negative” superhumps which occur on a period a few percent *shorter* than P_{orb} . This is believed to arise from precession of a disc warp and we will not consider these in this paper.

The intent of this paper is to test our understanding of the (positive) superhump phenomenon by comparing observation to the predictions of theoretical expressions for P_{sh} .

2 Pearson

Since this is directly observable, if we can relate it to the fundamental parameters of a system, we will have a method to indirectly measure such parameters.

2 THEORETICAL BACKGROUND

Lubow (1991a,b, 1992) derived the final precession rate ω for an eccentric disc as the sum of three terms:

$$\omega = \omega_{\text{dyn}} + \omega_{\text{press}} + \omega_{\text{tran}} \quad (3)$$

where ω_{dyn} is the dynamical precession frequency, ω_{press} is a pressure related term and ω_{tran} is a transient term. This latter contribution is related to the time derivative of the mode giving rise to the dynamical precession. Thus, it may be important in the development phase of the superhumps but not in steady state. As a result, we shall not consider it in detail except to note that it can have either sign and thus can either act to increase or decrease the precession rate.

The dynamical term is the one arising from the resonance and is examined in section 2.1. The pressure term acts to slow the precession and it is summarised in section 2.2.

2.1 Dynamical Precession Theory

Hirose & Osaki (1990) derived the general expression for the ratio of the dynamical disc precession ω_{dyn} and orbital ω_{orb} frequencies in terms of the mass ratio and radius of disc material. Their equation (8) is

$$\frac{\omega_{\text{dyn}}}{\omega_{\text{orb}}} = \frac{q}{(1+q)^{\frac{1}{2}}} \left[\frac{1}{2r^{\frac{1}{2}}} \frac{d}{dr} \left(r^2 \frac{dB_0}{dr} \right) \right] \quad (4)$$

where

$$B_0(r) = \frac{1}{2} b_{\frac{1}{2}}^0 = F \left(\frac{1}{2}, \frac{1}{2}, 1, r^2 \right) \quad (5)$$

(Brumberg 1995) is the zeroth order Laplace coefficient given in terms of the hypergeometric function F , $q = M_2/M_1$ (< 1) is the mass-ratio and r is the radius of orbiting material expressed as a fraction of the separation d . This evaluates to

$$\frac{\omega_{\text{dyn}}}{\omega_{\text{orb}}} = \frac{3}{4} \frac{q}{(1+q)^{\frac{1}{2}}} r^{\frac{3}{2}} \sum_{n=1}^{\infty} a_n r^{2(n-1)} \quad (6)$$

where the coefficients are given by

$$a_n = \frac{2}{3} (2n)(2n+1) \prod_{m=1}^n \left(\frac{2m-1}{2m} \right)^2 \quad (7)$$

(Pearson 2003). Lubow (1992) used the fixed value of $r = 0.477$ enigmatically described as ‘‘corrected for the presence of the companion’’ and thus presumably in the limit of $q \rightarrow 0$. Frank et al. (1992), however, give the radius for $j:j-1$ resonances as,

$$r_j = \frac{1}{j^{\frac{2}{3}} (1+q)^{\frac{1}{3}}}. \quad (8)$$

This evaluates to $r=0.481$ for the case of $j = 3$ and vanishing q ; very close to the value of the other paper but retaining accuracy for $q \neq 0$. Substituting into (6) gives

$$\frac{\omega_{\text{dyn}}}{\omega_{\text{orb}}} = \frac{3}{4j} \frac{q}{1+q} \sum_{n=1}^{\infty} \frac{a_n}{[j^2(1+q)]^{\frac{2(n-1)}{3}}}. \quad (9)$$

The canonical approximation

$$P_{\text{dyn}} \approx \frac{3.85(1+q)}{q} P_{\text{orb}} \quad (10)$$

(Warner 1995), is recovered by setting $j = 3$ and evaluating the summation with $q = 0.16$. The limiting mass ratio $q \approx 0.22$ found by Whitehurst (1988a) arises from the largest value for which r_3 remains within the last stable stream line (Molnar & Koblunicky 1992). Numerical simulations, however, still produce identifiable superhumps up to a mass ratio of $q \approx 0.33$ (Whitehurst 1994; Murray et al. 2000). Whitehurst (1991) used an approximation for the disc tidal radius

$$R_T \approx \beta R_{L,1} \quad (11)$$

with $\beta \approx 0.9$. When coupled to Eggleton’s formula (Eggleton 1983) for the primary’s Roche lobe radius

$$R_{L,1} = \frac{0.49q^{-\frac{2}{3}}}{0.6q^{-\frac{2}{3}} + \ln(1+q^{-\frac{1}{3}})} \quad (12)$$

$$\equiv E(q^{-1}) \quad (13)$$

and equated to the 3:2 resonance radius in equation (8), this gives a limiting mass ratio of $q_{\text{max}} = 0.28$, although this is sensitive to the choice of β . It should be noted, however, that this differs from the often cited value of $q_{\text{max}} = 0.33$ quoted in that paper, as equation (5) there contains an incorrect power of q . A slightly less *ad hoc* expression for the tidal radius comes from fitting to the simulations of Paczyński (1977)

$$R_T = \frac{0.60}{1+q} \quad 0.03 < q < 1. \quad (14)$$

Equating this to equation (8) gives a limiting mass ratio of

$$q = (0.6)^{\frac{3}{2}} j - 1 \quad (15)$$

which sets a maximum $q_{\text{max}} = 0.39$ for a 3:2 resonance.

2.2 Pressure Contribution

Lubow (1992) showed that the pressure term can be expressed as

$$\omega_{\text{press}} = -\frac{k^2 c^2}{2\omega_p} \quad (16)$$

where ω_p is the angular orbital frequency of a parcel of gas in the disc, k is the radial wavenumber of the mode and c is the gas sound speed. Clearly the pressure term acts in the opposite, retrograde sense to the dynamical term. For a spiral wave, the pitch angle i is related to k by

$$\tan i = \frac{1}{kr}. \quad (17)$$

From the resonance condition (eg. Warner 1995, eqn. 3.37), we have

$$(j-1)(\omega_p - \omega) = j(\omega_p - \omega_{\text{orb}}) \quad (18)$$

which becomes, when $\omega \ll \omega_{\text{orb}}$,

$$\omega_p = j\omega_{\text{orb}}. \quad (19)$$

Hence, for the 3:2 resonance $\omega_p = 3\omega_{\text{orb}}$. For the fixed radius $r = 0.477$, Montgomery (2001) corrected earlier errors to derive a contribution

$$\omega_{\text{press}} = -0.7325\omega_{\text{orb}} \left(\frac{c}{\omega_{\text{orb}}d} \frac{1}{\tan i} \right)^2. \quad (20)$$

For our general case using (19) and where r is given by equation (8), we have

$$\omega_{\text{press}} = -\frac{j^{\frac{1}{3}}}{2}(1+q)^{\frac{2}{3}}\omega_{\text{orb}} \left(\frac{c}{\omega_{\text{orb}}d} \frac{1}{\tan i} \right)^2. \quad (21)$$

To proceed further, we need to understand the behaviour of the final dimensionless term in brackets. Since values for c and i may vary according to the peculiar characteristics of any particular system, we will examine this in more detail in section 3.2.

3 COMPARISON

Observers normally present their measurements of the precession period in terms of the period excess

$$\epsilon = \frac{P_{\text{sh}} - P_{\text{orb}}}{P_{\text{orb}}} \quad (22)$$

or equivalently (noting $\omega_{\text{sh}} = \omega_{\text{orb}} - \omega$)

$$\epsilon = \frac{\omega}{\omega_{\text{orb}} - \omega} \quad (23)$$

$$= \left[\left(\frac{\omega_{\text{dyn}} + \omega_{\text{press}}}{\omega_{\text{orb}}} \right)^{-1} - 1 \right]^{-1} \quad (24)$$

$$\approx \frac{\omega_{\text{dyn}} + \omega_{\text{press}}}{\omega_{\text{orb}}} \quad \text{if } \omega_{\text{dyn}}, \omega_{\text{press}} \ll \omega_{\text{orb}}. \quad (25)$$

Since there are relatively few systems with accurately measured values of q , it is often convenient to make use of the theoretical relation

$$M_2 \approx 0.11P_{\text{orb}} \quad (26)$$

(Frank et al. 1992) that follows from the assumption that the secondary has a main sequence structure or an observationally derived equivalent

$$M_2 = (0.038 \pm 0.003)P_{\text{orb}}^{1.58 \pm 0.09} \quad (27)$$

(Smith & Dhillon 1998). In both cases M is measured in solar masses and P_{orb} in hours.

3.1 Dynamical precession only

For different assumed values of M_1 we can plot theoretically predicted lines on the ϵ - P_{orb} plane. Murray (2000) used equation 6 with the fixed radius value given by Lubow (1992) to compare the observed distribution with theory in just this way. He concluded that ‘‘superhumps observations cannot be adequately explained in terms of purely dynamical precession’’. However, including the q dependence of r given in equation 9 leads us to a different conclusion. Figure 1 reproduces the comparison of Murray (2000) using both methods. The lines are plotted for $M_1 = 0.76$, 0.76 ± 0.22 and $M_1 = 1.44$. This shows that the distribution is compatible with the boundary imposed by the condition $M_{\text{wd}} < 1.44$ when the full q dependence is included. In fact, the most we

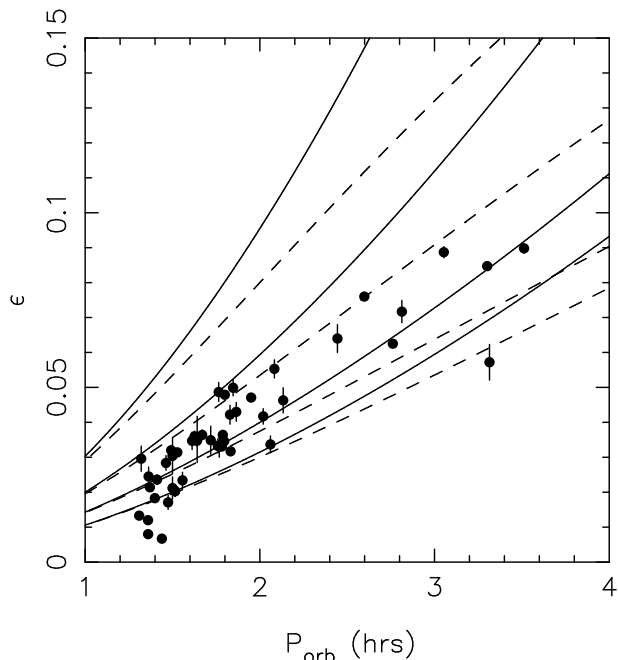


Figure 1. Comparison of the observed superhump data from Patterson (1998) with the model from Murray (2000), where the resonant radius is independent of q (solid), and with a model including the q dependence (dashed). Both family of curves show the theoretical lines derived using the mean (0.76) and $\pm 1\sigma$ (± 0.22) values for M_1 of all CVs and in the M_2 - P_{orb} relation (equation 27) from Smith & Dhillon (1998) as well as a further line with $M_1 = 1.44$. ϵ decreases with increasing M_1 . The turn to lower ϵ at $P_{\text{orb}} < 1.4$ may arise from the secondary becoming degenerate and deviating from a main sequence structure as assumed for the theoretical curves.

can conclude is that the distribution of superhumping systems suggests that they have a primary mass higher than the general CV population. This would not be entirely surprising since to be a superhumping system requires a small mass ratio and will thus tend to select higher M_1 systems. Also apparent is the deviation of the secondary from a main sequence structure at the short period turnoff.

More convincing evidence for the need for a pressure related effect on the precession rate is provided by the data for ϵ and q plotted in Figure 2. The 11 systems on this plot are those used in Patterson et al. (2005). These have directly determined values of q . The exception is OY Car which appears in Fig. 9 of that paper but not in the corresponding Table 7. We take the values for this system from Patterson (2001). We can see that the data are certainly not compatible with the assumption of a 3:2 resonance. If anything, they cluster around the prediction for a 4:3 resonance, although given the way the resonances ‘pile up’ one can argue that it is inevitable that some resonance would fall near the data. It is intriguing to note however, just how close the two most accurately measure values of q for the systems XZ Eri and DV UMA (Feline et al. 2004) lie to the 4:3 theoretical line (see Figure 3). It would thus be extremely interesting to see modelling using the method employed by these authors applied to the other eclipsing systems to determine similarly accurate values for q . We summarise the χ^2 value for the data against each resonance in Table 3.1 and note the

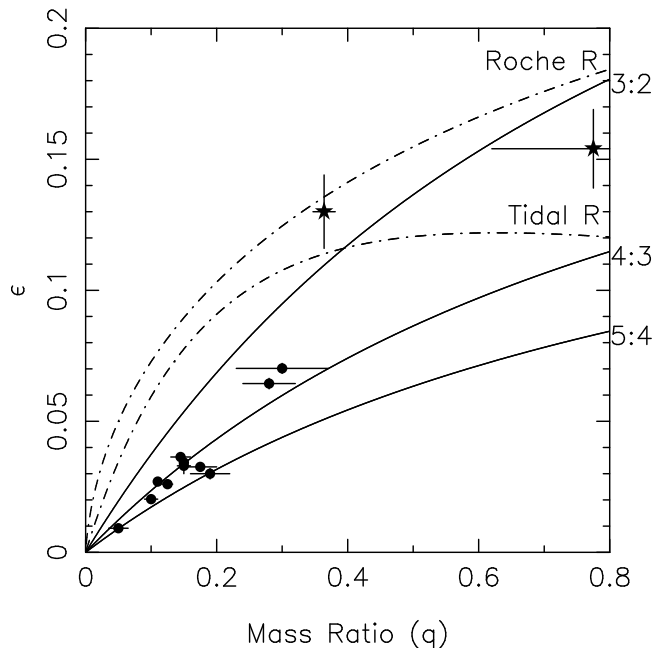


Figure 2. Comparison of the observed superhump data from Patterson et al. (2005) (circles), for systems with accurately measured values of q , and the dynamical precession rates of discs with radii calculated under different assumptions. The resonance period excesses are calculated using equation (9) and the discs with radii equal to the tidal and (unphysically) the Roche lobe radius are calculated using equation (6). The stars mark the additional ‘challenging’ systems U Gem and TV Col.

Resonance	$\frac{\chi^2}{N_{\text{Obs}}}$
3:2	49.5
4:3	1.28
5:4	18.9

Table 1. Summary of the χ^2 statistic comparing purely dynamical resonant precession to the observed period excess.

remarkable reduction in χ^2 for the 4:3 model. If a purely dynamical 4:3 resonance were the correct model, the probability that the value of χ^2 would exceed the measured value is 0.23.

We have followed the precedent of Patterson et al. (2005) in the systems considered above but we mention here briefly two further systems: U Gem and TV Col. On the grounds that U Gem does not show superhumps, Patterson et al. (2005) used its observed mass ratio to place an upper limit on the system BB Dor which does have measured period excess. However, Smak & Waagen (2004) reported the detection of superhumps in the 1984 outburst of U Gem. As a result, we dropped BB Dor from the analysis. Similarly, Retter et al. (2003) report a superhump detection near the expected 6.3-h in TV Col from an exhaustive search in archival and from fresh 2001 observations. Two other campaigns, however, failed to confirm this result (Patterson et al. 2005). Neither U Gem nor TV Col fit comfortably within the context of the precessing disc theory

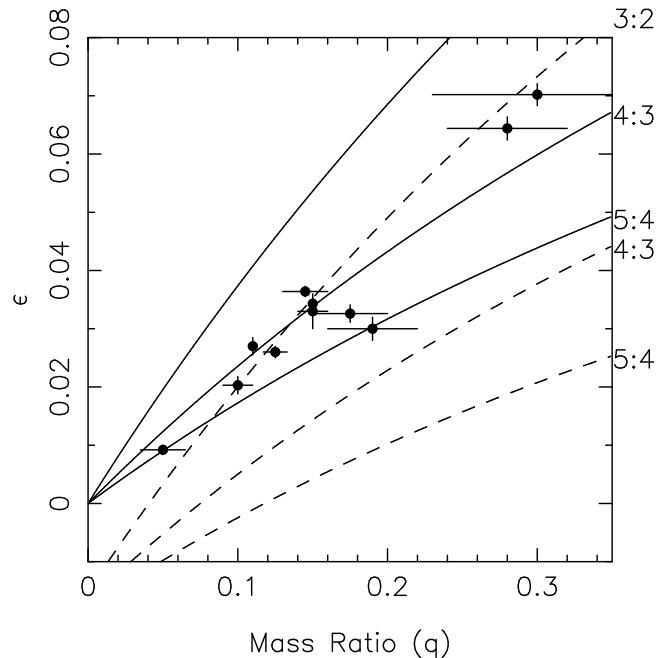


Figure 3. A closer view of the data used in the comparison of the observed superhump data from Patterson et al. (2005), for systems with accurately measured values of q , and the dynamical precession rates of discs at resonant radii (solid line). Also plotted are the model lines including an approximation to pressure effect (Model A; dashed line).

set out above. However, both have noticeably large errors on the value of their period excess. In the case of U Gem this reflects a systematic trend as the putative superhump period drifted to longer values over time. The outburst was also notable for its unusual length and completely out of character for the system. To reach the observed period excess would require the disc to extend beyond the tidally truncated radius, which is not impossible for a disc of finite viscosity (Lynden-Bell & Pringle 1974; Papaloizou & Pringle 1977), but is uncomfortably close to the value we would get if the disc had a radius equal to that of the primary’s entire Roche lobe! The most plausible explanation for such a large period excess and the unusual character is that the transient term ω_{tran} has become important and that the change in the observed period excess reflects a change in the rate of growth of the disc eccentricity. The uncertainties in the values for TV Col make it a difficult system to assess. The expected disc radius is again much larger than the tidal truncation radius and in addition to the large range of allowed q there is the possibility of unknown systematic errors due to the multiple components of the emission lines (Hellier 1993). We thus neglect this system also but echo the call of Retter et al. (2003) for a search for permanent superhumps in similarly long period systems.

Despite the encouraging agreement with a 4:3 resonance there are several theoretical hurdles to overcome before we could accept such an explanation. The theory outlined in Section 2 is only a summary of the extensive literature in this area (eg Goldreich & Tremaine (1978, 1979); Borderies, Goldreich & Tremaine (1983)). In outline, the

System	$\frac{r_{\text{eff}}}{r_3}$
WZ Sge	0.718
OY Car	0.770
XZ Eri	0.844
IY UMa	0.787
Z Cha	0.864
HT Cas	0.816
DV UMa	0.831
OU Vir	0.762
V2051 Oph	0.707
DW UMa	0.873
UU Aqr	0.886

Table 2. Values for r_{eff} derived from the observed period excesses for the Patterson et al. (2005) calibration systems.

analytical method employed is to decompose the effective potential into its harmonic components, to introduce this into the fluid equations in a standard linear perturbation analysis and to look at the response of the disc material. The behaviour of the disc in superhumping systems has a close analogue in galactic dynamics. The “dynamical resonance” above corresponds to the inner Lindblad resonance of the system and there is a similar result to that given, for example by Binney & Tremaine (1987), that leads to spiral waves being generated in the disc. It is these spiral waves that couple with the tides to excite disc eccentricity. There is also a corotational resonance that acts to suppress eccentricity.

Cursory consideration shows the fundamental contradiction of treating the dissipation arising from an eccentric disc (an inherently collective phenomenon) by the precession of single particle orbits at a resonant radius as carried out above. As a first attempt to correct for the untreated collective effects, we might assume that the precession can be characterised by an effective radius (r_{eff}) interior to r_3 that would produce dynamical precession with the observed period. The values for r_{eff} derived from the observed superhump period excesses of the Patterson et al. (2005) systems with well measured q are given in Table 3.1. Assuming that the ratio r_{eff}/r_3 is a constant for all systems, we derive a best value for it of 0.827. This places r_{eff} extremely close to r_4 with a barely different value for the total χ^2 . In fact, the radius calculated from a $j = 4$ resonance differs from this best possible radius by a suprisingly small 0.2%!

The above result notwithstanding, a treatment that deals explicitly with the coupling of the tides, spiral arms and disc eccentricity explicitly ought to be preferred. This is exactly the approach used by Lubow (1991a) to derive the additional term related to pressure effects which we turn to next. One of the important results from that paper was the recognition that the 3:2 resonance “is unique in that it is the innermost resonance for which an eccentric Lindblad resonance appears without an overlapping eccentric corotational resonance. . . This property allows that resonance to easily excite eccentricity.” Such a conclusion is a strong argument against any dynamical resonance other than 3:2 being an important factor in the disc behaviour. The ability of a secondary magnetic field to give rise to a precession rate characteristic of a higher resonance (Pearson, Wynn & King 1997; Pearson 2003) may reflect the fact that the perturbation in

that case is no longer small and capable of representation by a linear analysis.

3.2 Inclusion of Pressure Effects

Proceeding under the assumption that the excited resonance is 3:2 and that the difference between the measured and expected ϵ is due to the pressure effect we can update the analysis of Murray (2000) for all the systems with measured q . These are summarised in table 3.2. For the final column we have used values for M_1 from Patterson et al. (2005) except for V2051 Oph which we take from Ritter & Kolb (2003).

To make progress with our comparison we need values for c and i in equation 21. We will consider two cases: A) where $\frac{c \cot i}{\omega_{\text{orb}} d}$ is fixed for all systems and B) where c is evaluated using analytic expression taken from detailed disc models.

3.2.1 Model A

If we assume that the final bracketed term of equation (21) is constant we can rewrite it as

$$\frac{\omega_{\text{press}}}{\omega_{\text{orb}}} = -j^{\frac{1}{3}} \eta_A (1+q)^{\frac{2}{3}} \quad (28)$$

where

$$\eta_A = \frac{1}{2} \left(\frac{c \cot i}{\omega_{\text{orb}} d} \right)^2. \quad (29)$$

Lubow (1992) gave a range of 0.01–0.05 for the ratio $\frac{c}{\omega_{\text{orb}} d}$. Murray (2000) used a value of 0.05 in his considerations to derive values for i . Using this value and the mean $i = 17^\circ$ found from simulations by Montgomery (2001), we have $\eta_A = 0.0134$. Compared to the data for the eclipsing systems, this gives $\frac{\chi^2}{N_{\text{obs}}} = 3.3$. Allowing η_A to be a free parameter, however, we derive an optimal value of $\eta_A = 0.0107$ with a corresponding $\frac{\chi^2}{N_{\text{obs}}-1} = 1.42$. Figure 3 shows the comparison for this value in graphical form.

The corresponding plot to Figure 1, comparing a purely dynamical 3:2 resonance and a model including pressure, is shown in Figure 4. It should be noted here that the values assumed for M_1 in producing the lines come from the weighted mean derived by Smith & Dhillon (1998) for *dwarf nova* systems ($M_1 = 0.69 \pm 0.01$) rather than that for all systems used by Murray (2000). We have also updated the data to the latest compilation from Patterson et al. (2005). Coupling the mean primary mass with $q_{\text{max}} = 0.39$, we can derive an equivalent $P_{\text{orb,max}} = 3.5$ -h. For the ultimate restriction $M_1 < 1.44 M_\odot$ we have $P_{\text{orb,max}} = 5.5$ -h (coincidentally the same as that of TV Col).

We might like to compare the implied distribution of M_1 from our model with that of Smith & Dhillon (1998). However, this is precluded by the selection effect alluded to in section 3.1 being at work. Systems with longer periods (and thus higher M_2) can accommodate more massive primaries and still fit within the q_{max} limitation. Hence, the distribution of M_1 would be expected to differ between all dwarf novae and the superhumping subset. Figure 4 also shows systems lying above the limiting ϵ allowed by our formulation of the pressure term. This, along with the range of derived η_A shown in Table 3.2 and the poorer fit to the

System	ω (d ⁻¹)	ω_{dyn} (d ⁻¹)	ω_{press} (d ⁻¹)	$\sqrt{2\eta_A}$	$\frac{c}{\omega_{\text{orb}}d}$	c (10 ⁴ m s ⁻¹)
WZ Sge	1.01	2.13	-1.12	0.12	0.036	2.07
OY Car	1.98	3.59	-1.61	0.14	0.044	2.16
XZ Eri	2.70	4.02	-1.32	0.13	0.039	2.02
IY UMa	2.15	3.71	-1.56	0.15	0.047	2.29
Z Cha	2.96	4.17	-1.21	0.13	0.041	1.80
HT Cas	2.73	4.34	-1.62	0.15	0.047	2.14
DV UMa	2.43	3.73	-1.30	0.15	0.046	2.38
OU Vir	2.73	4.99	-2.26	0.18	0.055	2.87
V2051 Oph	2.93	6.20	-3.27	0.20	0.061	3.21
DW UMa	2.78	3.79	-1.01	0.16	0.049	1.99
UU Aqr	2.52	3.33	-0.81	0.16	0.048	1.78

Table 3. Derived pressure force contribution to the precession of the Patterson et al. (2005) calibration systems. The last two columns assume $i = 17^\circ$.

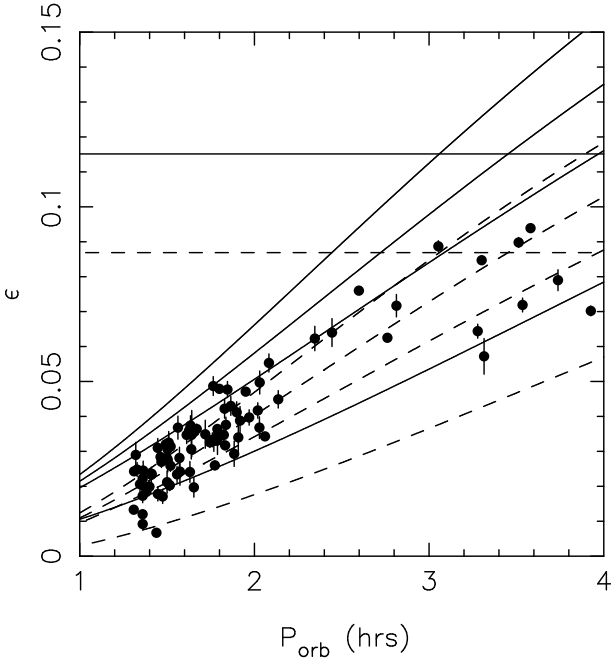


Figure 4. Comparison of the observed superhump data from Patterson et al. (2005) with a model with purely dynamical precession (solid) and including the pressure effect (dashed). Both family of curves show the theoretical lines derived using the mean (0.69) and $\pm 1\sigma$ (0.01) values for M_1 found for *dwarf novae* and in the M_2 - P_{orb} relation (equation 27) from Smith & Dhillon (1998) as well as a further line with $M_1 = 1.44$. ϵ decreases with increasing M_1 . The horizontal lines mark the limiting precession rate derived from $q_{\text{max}} = 0.39$ in either case.

data than a simple resonance model, suggests that a one size fits all value for η is not appropriate.

3.2.2 Model B

Since the effect of the pressure term relies on the sound speed in the disc, we turn to detailed models of hot discs to evaluate this in terms of fundamental parameters. From equation A1 of Cannizzo & Reiff (1992) we have the mid-plane temperature in terms of the mass transport rate through the disc

$$T_{\text{mid}} = \left(\frac{64}{9} \frac{\sigma}{\kappa_0}\right)^{-\frac{1}{10}} \left(\frac{\mu_{\text{H}}}{R}\right)^{\frac{1}{4}} \omega_{\text{p}}^{\frac{1}{2}} \alpha_{\text{H}}^{-\frac{1}{5}} \left(\frac{\dot{M}}{2\pi}\right)^{\frac{3}{10}} \quad (30)$$

where σ is the Stefan-Boltzman constant, R is the gas constant, α_{H} and μ_{H} are the Sunyaev-Shakura viscosity parameter and mean molecular weight in the hot state respectively and assuming an opacity $\kappa = \kappa_0 \rho T^{-3.5}$ where $\kappa_0 = 2.8 \times 10^{23} \text{ m}^2 \text{ kg}^{-1}$ is appropriate (Cannizzo, Shafer & Wheeler 1988). We can find a suitable value of \dot{M} for an outbursting dwarf nova using the approach of Cannizzo (1993) and Cannizzo, Shafer & Wheeler (1988) by assuming that the disc fills to a mass fM_{max} . M_{max} is the maximum mass the disc can hold in the cold state without exceeding Σ_{max} at some point ie.

$$fM_{\text{max}} = f \int_0^{r_{\text{d}}} 2\pi r \Sigma_{\text{max}}(r) dr \quad (31)$$

$$= f \frac{2\pi r_{\text{d}}^2}{3.05} \Sigma_{\text{max}}(r_{\text{d}}). \quad (32)$$

Now, equation A3 of Cannizzo & Reiff (1992) gives the surface density in the hot state as

$$\Sigma = \left(\frac{64}{9} \frac{\sigma}{\kappa_0}\right)^{\frac{1}{10}} \left(\frac{\mu_{\text{H}}}{R}\right)^{\frac{3}{4}} \omega_{\text{p}}^{\frac{1}{2}} \alpha_{\text{H}}^{\frac{4}{5}} \left(\frac{\dot{M}}{2\pi}\right)^{\frac{7}{10}} \quad (33)$$

$$= 405 \text{ kg m}^{-2} \mu_{\text{H}}^{\frac{3}{4}} \alpha_{\text{H}}^{-\frac{4}{5}} M_1^{\frac{1}{4}} \left(\frac{r}{10^8 \text{ m}}\right)^{-\frac{3}{4}} \times \left(\frac{\dot{M}}{10^{-10} M_{\odot} \text{ y}^{-1}}\right)^{\frac{7}{10}} \quad (34)$$

where we have used $\omega_{\text{p}} = (GM_1 M_{\odot} r^{-3})^{\frac{1}{2}}$. Integrating this and equating it to the expression for fM_{max} from (32), we can rearrange for the mass transport rate through the disc

$$\begin{aligned} \dot{M} &= 9.67 \times 10^{-8} \text{ kg s}^{-1} \left(\frac{\alpha_{\text{H}}}{0.1}\right)^{1.14} \left(\frac{\alpha_{\text{C}}}{0.02}\right)^{-1.23} \mu_{\text{H}}^{-1.07} \\ &\quad \times r_{\text{d}}^{2.57} M_1^{-0.86} \left(\frac{f}{0.4}\right)^{1.43} \end{aligned} \quad (35)$$

which, with equation (30), gives

$$\begin{aligned} c^2 &= \frac{\gamma k T}{\mu_{\text{H}} m_{\text{H}}} \\ &= 5.66 \times 10^4 \text{ m}^{1.229} \text{ s}^{-\frac{3}{2}} \left(\frac{\alpha_{\text{H}}}{0.1}\right)^{0.142} \left(\frac{\alpha_{\text{C}}}{0.02}\right)^{-0.369} \end{aligned} \quad (36)$$

$$\times \mu_{\text{H}}^{-1.071} r_{\text{d}}^{0.771} M_1^{-0.258} \left(\frac{f}{0.4}\right)^{0.429} \omega_p^{\frac{1}{2}}. \quad (37)$$

Finally, we can combine this with equations (8), (16), (17) and (19) to get

$$\begin{aligned} \frac{\omega_{\text{press}}}{\omega_{\text{orb}}} &= -2.83 \times 10^4 j^{\frac{5}{6}} (1+q)^{\frac{2}{3}} \cot^2 i \left(\frac{\alpha_{\text{H}}}{0.1}\right)^{0.142} \\ &\times \left(\frac{\alpha_{\text{C}}}{0.02}\right)^{-0.369} \mu_{\text{H}}^{-1.071} r_{\text{d}}^{0.771} M_1^{-0.258} \\ &\times \left(\frac{f}{0.4}\right)^{0.429} \omega_{\text{orb}}^{-\frac{3}{2}}. \end{aligned} \quad (38)$$

Since we want an expression for ω_{press} in terms of q only, we look to eliminate ω_{orb} by using a form of the mass-radius relation recommended by Smith & Dhillon (1998)

$$\frac{R_2}{R_{\odot}} = (0.91 \pm 0.09) M_2^{0.75 \pm 0.04}. \quad (39)$$

When this is equated to the size of the secondary's Roche lobe from (13), we can rearrange for the separation

$$d = \frac{0.91 M_2^{0.75} R_{\odot}}{E(q)}. \quad (40)$$

Using this with Kepler's Law

$$\omega_{\text{orb}} = [GM_1(1+q)M_{\odot}]^{\frac{1}{2}} d^{-\frac{3}{2}} \quad (41)$$

and a disc radius $r_{\text{d}} = \beta R_{\text{L},1}$, we arrive at the final expression

$$\frac{\omega_{\text{press}}}{\omega_{\text{orb}}} = -j^{\frac{5}{6}} \eta_{\text{B}} \frac{[E(q^{-1})]^{0.771} q^{0.766}}{[E(q)]^{1.021} (1+q)^{\frac{1}{12}}} \quad (42)$$

where

$$\begin{aligned} \eta_{\text{B}} &= 0.0209 \cot^2 i \left(\frac{\alpha_{\text{H}}}{0.1}\right)^{0.142} \left(\frac{\alpha_{\text{C}}}{0.02}\right)^{-0.369} \\ &\times \mu_{\text{H}}^{-1.071} \left(\frac{f}{0.4}\right)^{0.429} \left(\frac{\beta}{0.9}\right)^{0.771} M_1^{-0.242}. \end{aligned} \quad (43)$$

Hence, we can see that although the pressure term is not purely expressible as a function of q alone, the various parameters are either expected to remain reasonably constant between systems (eg. μ_{H}) or enter in with a weak dependency such as $M_1^{-0.242}$. As mentioned above, the observed distribution for *all* CVs is $M_1 = 0.76 \pm 0.22$ which would produce a variation of only $\sim 7\%$ in the predicted pressure contribution. The dwarf nova subsample had an even smaller range for M_1 .

The final expression for the precession rate was fitted to the calibration systems of Patterson et al. (2005) using a single free parameter as the constant of proportionality to the functional form of q in (42). The best fitting value of $\eta_{\text{B}} = 0.0109$ gives $\frac{\chi^2}{N_{\text{obs}}-1} = 1.04$. With the typical values used above this implies $i = 61^\circ$. A comparison with the data is plotted in Figure 5. For the lowest q systems the effect of the pressure term actually makes ϵ negative, ie. force the precession to become retrograde.

Inverting the process for systems of known ϵ but unknown q allows us to derive values for the 88 systems in Table 9 of Patterson et al. (2005). These are listed in Table 3.2.2. The errors quoted in the table reflect the observational errors propagated as appropriate but not the systematic errors that may arise from variations of the parameters in the Smith & Dhillon (1998) relations. It is apparent that

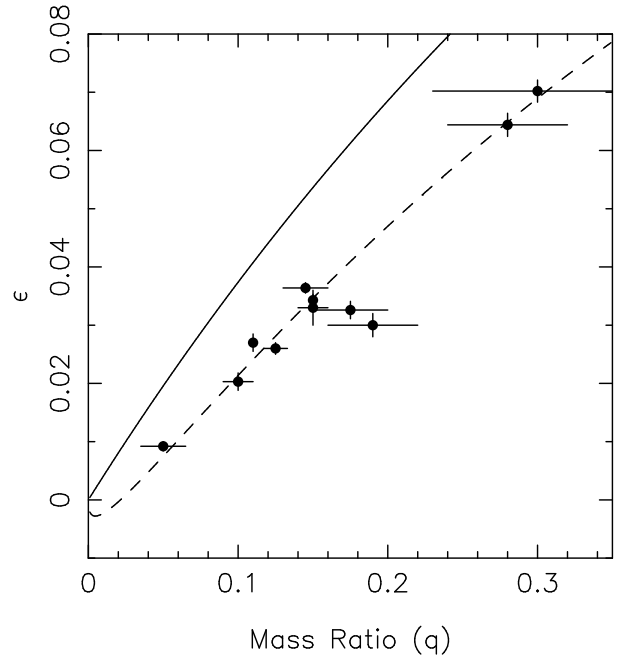


Figure 5. Comparison of the calibration systems from Patterson et al. (2005) with a model with purely dynamical precession (solid) and including the detail pressure term in equation (42) (dashed).

some systems have predicted values of q in excess of the expected limit of $q_{\text{max}} = 0.28$ for $\beta = 0.9$. The largest derived value of $q = 0.437$ can be accommodated if $\beta = 0.94$. If the resonance were to transition to 4:3 at some q_{max} , the derived values of q would be even higher. However, axisymmetric structure models were used in the above derivation. As r_j approaches R_{T} this will become an increasingly invalid assumption. It might be reasonably expected then that these high q systems have true mass ratios close to q_{max} although, as we have seen, this limit is not well determined.

It is also worth noting just how close is the derived M_1 in EG Cnc to the Chandrasekhar limit. Although the mass-period relation we have used (equation 39) was derived from observations, there are strong theoretical grounds for expecting a significantly different relation for the lowest mass secondaries once they become degenerate or semi-degenerate. EG Cnc is towards the low-end in the range of M_2 where this effect may be important and we may be extrapolating the relation beyond its range of validity. A non-main-sequence star would be expected to have a larger radius for the same mass as a main-sequence equivalent. This would lead to a larger pressure effect for a given value of q . As a result we would tend to underestimate both M_2 and q when such deviation becomes important. In principle, analytic forms for the mass-radius relations for the appropriate ranges of M_2 could be included in place of (39).

As a disc outburst proceeds, we would expect \dot{M} to steadily decrease. Since $c^2 \propto \dot{M}^{\frac{3}{10}}$ this would cause the pressure term to also shrink and thus the period excess to increase during an outburst. Observationally, the opposite appears to be the case, with the period excess decreasing with time (Patterson et al. 1993). The only available param-

Name	$P_{\text{orb}}(\text{d})$	ϵ	q	M_2	M_1
DI UMa	0.05456(1)	0.0133(6)	0.071(2)	0.058	0.821(25)
V844Her	0.05464(1)	0.0243(9)	0.111(3)	0.058	0.526(16)
LLAND	0.05505(1)	0.0290(36)	0.128(14)	0.059	0.459(49)
SDSS0137-09	0.05537(4)	0.0248(20)	0.113(7)	0.060	0.528(35)
ASAS0025+12	0.05605(5)	0.0206(21)	0.097(8)	0.061	0.624(49)
AL Com	0.05667(3)	0.0120(7)	0.066(3)	0.062	0.933(35)
WZ Sge	0.05669(1)	0.0092(7)	0.056(3)	0.062	1.100(49)
RX1839+26	0.05669(5)	0.0173(20)	0.085(7)	0.062	0.724(61)
PU CMa	0.05669(5)	0.0222(20)	0.103(7)	0.062	0.599(43)
SW UMa	0.05681(14)	0.0245(27)	0.112(10)	0.062	0.556(50)
HV Vir	0.05707(1)	0.0200(9)	0.095(3)	0.062	0.657(23)
MM Hya	0.05759(1)	0.0184(10)	0.089(4)	0.063	0.710(29)
WX Cet	0.05829(4)	0.0199(15)	0.095(5)	0.065	0.682(39)
KV Dra	0.05876(7)	0.0233(22)	0.107(8)	0.065	0.610(46)
T Leo	0.05882(1)	0.0236(14)	0.108(5)	0.066	0.605(29)
EG Cnc	0.05997(9)	0.0067(8)	0.047(3)	0.068	1.433(88)
V1040 Cen	0.06028(10)	0.0310(27)	0.136(10)	0.068	0.501(38)
RX Vol	0.06030(20)	0.0178(20)	0.087(7)	0.068	0.782(65)
AQ Eri	0.06094(6)	0.0284(21)	0.126(8)	0.069	0.549(34)
XZ Eri	0.06116(1)	0.0270(16)	0.121(6)	0.070	0.576(28)
CP Pup	0.06145(6)	0.0171(20)	0.085(7)	0.070	0.830(71)
V1159 Ori	0.06218(1)	0.0320(11)	0.140(4)	0.072	0.512(15)
V2051 Oph	0.06243(1)	0.0281(25)	0.125(9)	0.072	0.576(43)
V436 Cen	0.06250(20)	0.0212(32)	0.099(12)	0.072	0.725(85)
BC UMa	0.06261(1)	0.0306(14)	0.134(5)	0.072	0.538(21)
HO Del	0.06266(16)	0.0276(35)	0.123(13)	0.072	0.588(63)
EK TrA	0.06288(5)	0.0321(25)	0.140(10)	0.073	0.519(35)
TV Crv	0.06290(20)	0.0325(32)	0.142(12)	0.073	0.513(44)
VY Aqr	0.06309(4)	0.0203(15)	0.096(5)	0.073	0.761(43)
OY Car	0.06312(1)	0.0203(15)	0.096(5)	0.073	0.761(43)
RX1131+43	0.06331(8)	0.0259(16)	0.117(6)	0.074	0.630(32)
ER UMa	0.06336(3)	0.0314(11)	0.138(4)	0.074	0.536(17)
DM Lyr	0.06546(6)	0.0281(31)	0.125(12)	0.078	0.620(58)
UV Per	0.06489(11)	0.0234(23)	0.108(8)	0.077	0.711(56)
AK Cnc	0.06510(20)	0.0368(33)	0.158(13)	0.077	0.486(40)
AO Oct	0.06557(13)	0.0242(39)	0.111(14)	0.078	0.704(92)
SX LMi	0.06717(11)	0.0347(25)	0.150(10)	0.081	0.538(35)
SS UMi	0.06778(4)	0.0360(15)	0.155(6)	0.082	0.528(20)
KS UMa	0.06796(10)	0.0241(30)	0.110(11)	0.082	0.747(75)
V1208 Tau	0.06810(20)	0.0374(28)	0.161(11)	0.083	0.514(35)
RZ Sge	0.06828(2)	0.0306(28)	0.134(11)	0.083	0.617(49)
TY Psc	0.06833(5)	0.0347(15)	0.150(6)	0.083	0.553(21)
IR Gem	0.06840(30)	0.0351(66)	0.152(26)	0.083	0.548(93)
V699 Oph	0.06890(20)	0.0197(28)	0.094(10)	0.084	0.895(97)
CY UMa	0.06957(4)	0.0364(14)	0.157(5)	0.085	0.545(19)
FO And	0.07161(18)	0.0349(40)	0.151(16)	0.089	0.592(61)
OU Vir	0.07271(1)	0.0326(15)	0.142(6)	0.092	0.643(26)
VZ Pyx	0.07332(3)	0.0333(20)	0.145(8)	0.093	0.641(34)
CC Cnc	0.07352(5)	0.0487(27)	0.207(11)	0.093	0.449(25)
HT Cas	0.07365(1)	0.0330(30)	0.144(12)	0.093	0.651(52)
IY UMa	0.07391(1)	0.0260(13)	0.117(5)	0.094	0.802(33)
VW Hyi	0.07427(1)	0.0331(8)	0.144(3)	0.095	0.658(13)
Z Cha	0.07450(1)	0.0364(9)	0.157(4)	0.095	0.607(14)
QW Ser	0.07453(10)	0.0331(40)	0.144(15)	0.095	0.661(71)
WX Hyi	0.07481(1)	0.0346(14)	0.150(5)	0.096	0.639(23)
BK Lyn	0.07498(5)	0.0479(7)	0.204(3)	0.096	0.471(7)
RZ Leo	0.07604(1)	0.0347(25)	0.150(10)	0.098	0.654(42)
AW Gem	0.07621(10)	0.0422(27)	0.180(11)	0.099	0.548(33)
SU UMa	0.07635(5)	0.0317(12)	0.139(5)	0.099	0.713(23)

Table 4. Derived parameters for all the systems with measured period excesses from Patterson et al. (2005). The errors on q reflect the observational errors propagated appropriately. M_2 has been calculated using equation (27) and $M_1 = \frac{q}{M_2}$. No allowance has been made for the systematic error that would arise from the errors in the parameters in this relation. Similarly, no error is quoted for M_2 since this is dominated by the assumption of main sequence structure.

Star	$P_{\text{orb}}(\text{d})$	ϵ	q	M_2	M_1
SDSS1730+62	0.07655(9)	0.0376(22)	0.162(9)	0.099	0.615(33)
HS Vir	0.07690(20)	0.0477(23)	0.203(10)	0.100	0.493(23)
V503 Cyg	0.07770(20)	0.0430(27)	0.183(11)	0.102	0.555(34)
V359 Cen	0.07990(30)	0.0388(40)	0.166(16)	0.106	0.639(61)
CU Vel	0.07850(20)	0.0293(36)	0.130(14)	0.103	0.798(83)
NSV 9923	0.07910(20)	0.0412(30)	0.176(12)	0.105	0.595(41)
BR Lup	0.07950(20)	0.0340(40)	0.147(15)	0.105	0.716(75)
V1974 Cyg	0.08126(1)	0.0471(10)	0.201(4)	0.109	0.544(11)
TU Crt	0.08209(9)	0.0397(22)	0.170(9)	0.111	0.653(34)
TY PsA	0.08414(18)	0.0417(22)	0.178(9)	0.115	0.648(32)
KK Tel	0.08453(21)	0.0368(31)	0.158(12)	0.116	0.734(56)
V452 Cas	0.08460(20)	0.0497(33)	0.212(14)	0.116	0.550(37)
DV Uma	0.08585(1)	0.0343(11)	0.149(4)	0.119	0.801(23)
YZ Cnc	0.08680(20)	0.0553(26)	0.236(12)	0.121	0.514(25)
GX Cas	0.08902(16)	0.0449(25)	0.191(11)	0.126	0.660(37)
NY Ser	0.09775(19)	0.0623(35)	0.268(16)	0.146	0.546(33)
V348 Pup	0.10184(1)	0.0640(40)	0.276(19)	0.156	0.565(39)
V795 Her	0.10826(1)	0.0760(10)	0.336(5)	0.172	0.512(8)
V592 Cas	0.11506(1)	0.0625(5)	0.269(2)	0.189	0.703(6)
TU Men	0.11720(20)	0.0717(32)	0.314(16)	0.195	0.621(32)
AH Men	0.12721(6)	0.0887(16)	0.406(9)	0.222	0.546(13)
DW Uma	0.13661(1)	0.0644(20)	0.278(10)	0.248	0.893(31)
TT Ari	0.13755(1)	0.0847(7)	0.383(4)	0.251	0.655(7)
V603 Aql	0.13810(20)	0.0572(51)	0.244(23)	0.252	1.032(97)
PX And	0.14635(1)	0.0898(14)	0.412(8)	0.277	0.671(13)
V533 Her	0.14730(20)	0.0719(20)	0.315(10)	0.279	0.888(29)
BB Dor	0.14920(10)	0.0939(10)	0.437(6)	0.285	0.652(9)
BH Lyn	0.15575(1)	0.0790(30)	0.352(16)	0.305	0.868(40)
UU Aqr	0.16358(1)	0.0702(14)	0.306(7)	0.330	1.077(25)

Table 4. Cont. Derived parameters for all the systems with measured period excesses from Patterson et al. (2005).

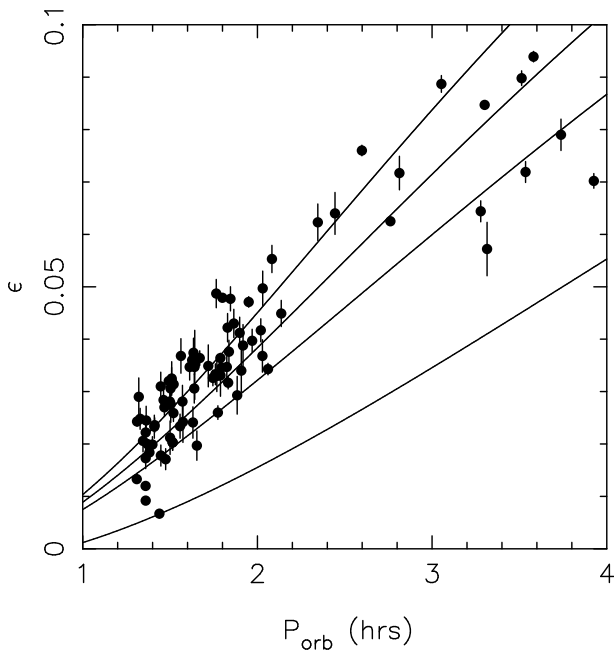


Figure 6. Comparison of the observed superhump data from Patterson et al. (2005) with a model including the full pressure effect. The curves use the mean (0.69) and $\pm 1\sigma$ (0.01) values for M_1 found for *dwarf novae* and in the M_2 - P_{orb} relation from Smith & Dhillon (1998) as well as a further line with $M_1 = 1.44$. ϵ decreases with increasing M_1 .

eter to counter this is $\tan i$ implying that the pitch angle i increases during an outburst.

Although the treatment of Lubow (1991a) includes the coupling of the tides, spiral waves and eccentricity, it shares the shortcoming of a purely dynamical resonance in that the properties are characterised by those at a single radius. A recent preprint of a paper by Goodchild & Ogilvie (2006) has addressed this problem with a detailed analysis solving the equations for the disc behaviour integrated over the whole range of disc radii. Their final equation describing the generation, damping and dynamics of eccentricity in the disc is

$$2r\Omega \frac{\partial E}{\partial t} = \frac{iE}{\rho} \frac{\partial p}{\partial r} + \frac{i}{r^2 \rho} \frac{\partial}{\partial r} \left((\gamma - i\alpha_b) p r^3 \frac{\partial E}{\partial r} \right) + \frac{i q \Omega^2 r^3}{2d^2} \left(b_{\frac{3}{2}}^1 \left(\frac{r}{d} \right) E \right) + 2\xi r \Omega E \delta(r - r_{\text{res}}). \quad (44)$$

Here E is the complex eccentricity $E = ee^{i\omega}$, p and ρ are the local disc pressure and density, $\gamma - i\alpha_b$ is a complex adiabatic exponent, $\xi = 2.08\omega_{\text{orb}} q^2 r_{\text{res}}$ is the eccentricity growth rate for a resonance at radius r_{res} from Lubow (1991a) and Ω is the angular velocity of the orbiting disc material. Unsurprisingly, the full solution has to be found numerically. These authors do so with undisturbed (vertically integrated) structure distributions given by

$$P = P_{\text{sc}} \left(\frac{r}{r_{\text{sc}}} \right)^{-\frac{3}{2}} \left(1 \sqrt{\frac{r_{\text{in}}}{r}} \right) \tanh \left(\frac{r_{\text{out}} - r}{\nu r_{\text{sc}}} \right) \quad (45)$$

$$\Sigma = \Sigma_{\text{sc}} \left(\frac{r}{r_{\text{sc}}} \right)^{-\frac{3}{4}} \left(1 \sqrt{\frac{r_{\text{in}}}{r}} \right)^{0.7} \tanh \left(\frac{r_{\text{out}} - r}{\nu r_{\text{sc}}} \right) \quad (46)$$

where r_{out} and r_{in} are the outer and inner radii disc radii and P_{sc} and Σ_{sc} are the pressure and surface density at the scaling radius r_{sc} . Considering the first bracketed terms in either case, the Cannizzo & Reiff (1992) equations used above have the same radial dependence. The second bracketed terms reflect the behaviour close to the inner radius. The final terms were chosen to implement the boundary conditions at the outer edge of the disc. Since we would expect the inner and outer terms to only become important close to the limiting mass ratios and given the similarity otherwise of the radial dependences of the equations to those used earlier, we do not need to repeat the integration here but compare the final results produced.

The results in Figure 8 of Goodchild & Ogilvie (2006) show a similar excursion to a negative period excess for small q . The curves also turn up to high ϵ as they asymptotically approach q_{max} which our expression does not produce. However, the turn off occurs very close to q_{max} for the best fitting curve and the details of the behaviour here depend on the functional form chosen to implement the boundary conditions for the outer edge of the disc in equations (45) and (46). Away from the extreme mass ratios the two sets of results are very close.

3.3 Empirical Fit

In an attempt to calibrate an empirical relation between ϵ and q , Patterson et al. (2005) extended the earlier fit of

$$\epsilon = 0.22q \quad (47)$$

(Patterson 2001) to

$$\epsilon = 0.18q + 0.29q^2. \quad (48)$$

We can view these as phenomenologically derived equivalents to the Maclaurin series for our analytic expression. Given the complexity of the full expressions, however, rather than carry out the necessary differentiation, it is simplest to generate $\epsilon(q)$ predictions from our formula numerically and then find the best fitting polynomial to these values using standard methods (Press et al. 1992). This approach gives an approximate formula

$$\epsilon = 3.5 \times 10^{-4} + 0.24q - 0.12q^2 \quad (49)$$

over the range $0.01 < q < 0.4$. This expression differs both with a very small constant offset and with a quadratic term that causes a curvature in the opposite sense to the empirical expression. This can be attributed to removing the q_{max} limitation imposed by U Gem for BB Dor. Goodchild & Ogilvie (2006) derive a best fit formula for their numerical integrations of (44) of

$$\epsilon = -4.1 \times 10^{-4} + 0.2076q. \quad (50)$$

These polynomial forms are compared graphically in Figure 7. The linear empirical fit, the full integration polynomial and our result all appear in good agreement.

4 SUMMARY

We have shown that the standard dynamical method of calculating the precession rate of superhumping CVs with a

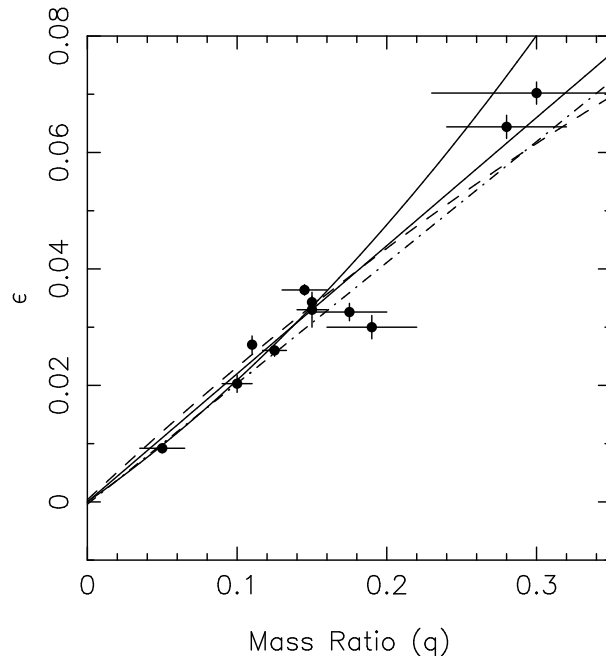


Figure 7. Comparison of the observed superhump data from Patterson et al. (2005) with the polynomial approximations for empirical fits (equations 47 and 48) (solid), this work (49) (dashed) and full integration (50) (dot-dashed).

3:2 provides such a poor fit to the data that a 4:3 resonance is actually a better fit! We have confirmed the importance of including the pressure related term in the calculation of the precession rate (Murray 2000) which fits the data better than any pure resonance model. The pressure term has been reduced to a function of q and the total, analytic precession rate shown to be equivalent to the empirically derived expressions of Patterson et al. (2005). These analytic expressions also produce precession rates in good agreement with those from the detailed integrations carried out by Goodchild & Ogilvie (2006). This formulation has been used to calculate values for q in systems which would otherwise be unknown.

ACKNOWLEDGEMENTS

I thank Robert Hynes and Juhan Frank for helpful remarks and advice regarding the work in this paper and the anonymous referee for insightful remarks that improved the presentation of these results.

REFERENCES

- Binney J., Tremaine S., 1987, *Galactic Dynamics*, Princeton University Press, Princeton
- Borderies N., Goldreich P., Tremaine S., 1983, *ApJ*, 88, 1560
- Brumberg V. A., 1995, *Analytical Techniques of Celestial Mechanics*, Springer Verlag, Berlin
- Cannizzo J. K., 1993, *ApJ*, 419, 318

- Cannizzo J. K., Shafter A. W., Wheeler J. C., 1988, ApJ, 333, 227
- Cannizzo J. K., Reiff C. M., 1992, ApJ, 385, 87
- Eggleton P. P., 1983, ApJ, 268, 368
- Feline W. J., Dhillon V. S., Marsh T. R., Brinkworth C. S., 2004, MNRAS, 355, 1
- Frank J., King A. R., Raine D. J., 1992, *Accretion Power in Astrophysics*, Cambridge Univ. Press.
- Goodchild P., Tremaine S., 1978, ApJ, 222,850
- Goodchild P., Tremaine S., 1979, ApJ, 223,857
- Goodchild S., Ogilvie G., 2006, MNRAS, in press (astro-ph/0602492)
- Hellier C., 1993, MNRAS, 264, 132
- Hirose M., Osaki Y., 1990, PASJ, 42, 135
- Lubow S. H., 1991a, ApJ, 381, 259
- Lubow S. H., 1991b, ApJ, 381, 268
- Lubow S. H., 1992, ApJ, 401, 317
- Lynden-Bell D., Pringle J. E., 1974, MNRAS, 168, 603
- Molnar L. A., Kobulnicky H. A., 1992, ApJ, 392, 678
- Montgomery M. M., 2001, MNRAS, 325, 761
- Murray J. R., 2000, MNRAS, 314, L1
- Murray J. R., Warner B., Wickramasinghe D. T., 2000, MNRAS, 707
- Paczyński B., 1977, ApJ, 216, 822
- Papaloizou J., Pringle J. E., 1977, MNRAS, 181, 441
- Patterson J., Bond H. E., Grauer A. D., Shafter A. W., Mattei J. A., 1993, PASP, 105, 69
- Patterson J., 1998, PASP, 110, 1132
- Patterson J., 2001, PASP, 113, 736
- Patterson J. et al., 2005, PASP, 117, 1204
- Pearson K. J., Wynn, G. A., King, A. R., 1997, MNRAS, 288, 421
- Pearson K. J., 2003, MNRAS, 346, L21
- Press W. H., Teukolsky S. A., Vetterling W. T., Flannery B. P., 1992, *Numerical Recipes in Fortran*, Cambridge Univ. Press, Cambridge, 2nd Edition
- Retter A., Naylor T., 2000, MNRAS, 319, 510
- Retter A. et al., 2003, MNRAS, 340, 679
- Ritter H., Kolb U., 2003, A&A, 404, 301
- Smak J., Waagen E. O., 2004, Acta Astron., 54, 433
- Smith D. A., Dhillon V. S., 1998, MNRAS, 301,767
- Warner B., 1995, *Cataclysmic Variable Stars*, Cambridge Univ. Press, Cambridge
- Whitehurst R., 1987, Ph.D. Thesis, Oxford Univ.
- Whitehurst R., 1988a, MNRAS, 232, 35
- Whitehurst R., 1994, MNRAS, 266, 35
- Whitehurst R., King A. R., 1991, MNRAS, 249, 25
- Zurita et al., 2002, MNRAS, 333, 791